minerals

MDPI

Article

A New Mineral Ferrisanidine, $K[Fe^{3+}Si_3O_8]$, the First Natural Feldspar with Species-Defining Iron

Nadezhda V. Shchipalkina [1,*], Igor V. Pekov [1], Sergey N. Britvin [2,3], Natalia N. Koshlyakova [1], Marina F. Vigasina [1] and Evgeny G. Sidorov [4]

[1] Faculty of Geology, Moscow State University, Vorobievy Gory, 119991 Moscow, Russia; igorpekov@mail.ru (I.V.P.); nkoshlyakova@gmail.com (N.N.K.); vigasina@geol.msu.ru (M.F.V.)
[2] Department of Crystallography, St Petersburg State University, University Embankment 7/9, St Petersburg 199034, Russia; sbritvin@gmail.com
[3] Nanomaterials Research Center, Kola Science Center of Russian Academy of Sciences, Fersman Str. 14, 184209 Apatity, Russia
[4] Institute of Volcanology and Seismology, Far Eastern Branch of Russian Academy of Sciences, Piip Boulevard 9, 683006 Petropavlovsk-Kamchatsky, Russia; mineral@kscnet.ru
* Correspondence: estel58@yandex.ru

Received: 10 November 2019; Accepted: 9 December 2019; Published: 11 December 2019

Abstract: Ferrisanidine, $K[Fe^{3+}Si_3O_8]$, the first natural feldspar with species-defining iron, is an analogue of sanidine bearing Fe^{3+} instead of Al. It was found in exhalations of the active Arsenatnaya fumarole at the Second scoria cone of the Northern Breakthrough of the Great Fissure Tolbachik Eruption, Tolbachik volcano, Kamchatka Peninsula, Russia. The associated minerals are aegirine, cassiterite, hematite, sylvite, halite, johillerite, arsmirandite, axelite, aphthitalite. Ferrisanidine forms porous crusts composed by cavernous short prismatic crystals or irregular grains up to 10 μm × 20 μm. Ferrisanidine is transparent, colorless to white, the lustre is vitreous. D_{calc} is 2.722 g·cm^{-3}. The chemical composition of ferrisanidine (wt. %, electron microprobe) is: Na_2O 0.25, K_2O 15.15, Al_2O_3 0.27, Fe_2O_3 24.92, SiO_2 60.50, in total 101.09. The empirical formula calculated based on 8 O *apfu* is $(K_{0.97}Na_{0.03})_{\Sigma 1.00}(Si_{3.03}Fe^{3+}_{0.94}Al_{0.02})_{\Sigma 3.99}O_8$. The crystal structure of ferrisanidine was studied using the Rietveld method, the final R indices are: R_P = 0.0053, R_{wp} = 0.0075, R_1 = 0.0536. Parameters of the monoclinic unit cell are: a = 8.678(4), b = 13.144(8), c = 7.337(5) Å, β = 116.39(8)°, V = 749.6(9) Å^3. Space group is $C2/m$. The crystal structure of ferrisanidine is based on the sanidine-type "ferrisilicate" framework formed by disordered $[SiO_4]$ and $[Fe^{3+}O_4]$ tetrahedra.

Keywords: ferrisanidine; new mineral; sanidine; feldspar group; iron in feldspar; crystal structure; fumarole; Tolbachik volcano; Kamchatka

1. Introduction

High content of iron is extremely rare for feldspar-group minerals. In most cases, the content of Fe_2O_3 in natural feldspars is not higher than 3 wt. % and all Fe-rich samples of minerals of this group belong to potassic feldspars [1,2]. The K-feldspar with distinct content of Fe_2O_3 (2.5–3.0 wt. %) was first described by Alfred Lacroix in 1912 from granitic pegmatites at Madagascar. Its optical properties are close to those of sanidine [3]. Fe-enriched (6.3 wt. % Fe_2O_3) potassic feldspar was described from manganese-rich skarns of the famous Långban deposit, Filipstad, Sweden [4]. "Sanidine" with 13.7 wt. % Fe_2O_3 and the empirical formula $(K_{0.95}Na_{0.03})[Si_{3.08}Fe^{3+}_{0.50}Al_{0.40}O_8]$ was reported by [5] from lamproites of Cancarix, Spain. Other researchers [6] published data on zoned crystals of sanidine with zones containing up to 18.4 wt. % Fe_2O_3 from leucite- and sanidine-bearing lavas of Leucite Hills, Wyoming, USA. The empirical formula of the most Fe-rich zone in these crystals is $(K_{0.96}Na_{0.04})_{\Sigma 1.00}[(Si_{3.02}Fe^{3+}_{0.70}Al_{0.20}Mg_{0.05}Ti_{0.03})_{\Sigma 4.00}O_8]$. In both these cases, an Fe-dominant (Fe >

Al in atom proportions) feldspar occurs as thin rims on sanidine crystals. However, no X-ray diffraction (XRD) data for natural samples of Fe-dominant feldspars were published and, therefore, nothing on crystallography of these minerals and the distribution of Si, Al and Fe in their crystal structures is known.

Unlike natural Fe-rich feldspars, synthetic ferri-feldspars are well-studied. The first experimental data revealing the possibility of Fe^{3+} presence in the feldspar-type crystal structure were obtained by [7], who synthesized so-called Fe-orthoclase. Later the investigation of the $KAlSi_3O_8$–$KFe^{3+}Si_3O_8$ solid-solution series and transitions between monoclinic and triclinic forms of $K[Fe^{3+}Si_3O_8]$ were the focus of many studies [8–13].

In this paper, we describe a natural feldspar chemically close to $KFe^{3+}Si_3O_8$ found in fumarole sublimates at the Tolbachik volcano, Kamchatka, Russia. This new mineral was named ferrisanidine as an analogue of sanidine with Fe^{3+} instead of Al. Both the new mineral and its name have been approved by the IMA Commission on New Minerals, Nomenclature and Classification, IMA No. 2019-052. The type specimen is deposited in the collection of the Fersman Mineralogical Museum of the Russian Academy of Sciences, Moscow, Russia, with catalogue number 96732.

2. Background Information: Crystal Structure and Nomenclature of Potassic Feldspars

Feldspar-type crystal structures are well-studied. Crystal chemistry of feldspars is described in many publications including several handbooks [1,2,14–16]. The feldspar structural archetype unites compounds with the general formula AT_4O_8. Until the present work, the species-defining constituents in valid feldspar-group minerals were as follows: tetrahedrally coordinated T = Si, Al, B, and As^{5+} and extra-framework cations A = Na, K, Rb, NH_4, Ca, Sr, and Ba.

The crystal structure of feldspars is based on a three-dimensional framework composed by corner-sharing TO_4 tetrahedra. The main structural unit is a chain of four-membered rings, called as "double crankshaft". These rings consist of tetrahedra T(1) and T(2) (in ordered species, T1O, T1m, T2O and T2m). The double crankshafts repeat throughout space by c-translations and are linked with one another as shown in Figure 1.

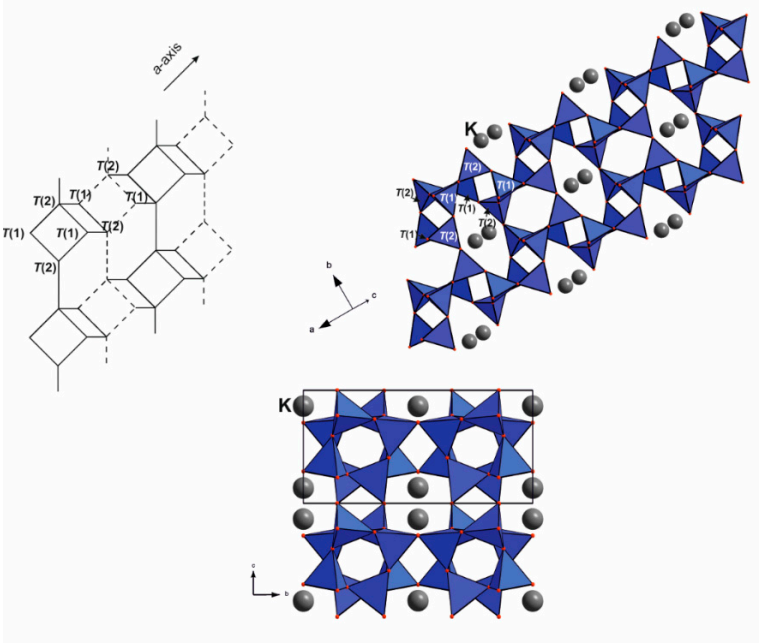

Figure 1. Two double-crankshaft chains parallel to the a axis in the crystal structure of ferrisanidine: the left figure is a schematic illustration of crankshaft chains where each line becomes a branch joining nodes, in which tetrahedrally coordinated T atoms located, of a four-connected net; the right figure is a projection of double-crankshaft chains parallel to the a axis with outlined TO_4 tetrahedra and K atoms; the lower figure displays the projection of the ferrisanidine crystal structure along the a axis.

The extra-framework *A* cations are located in the interstices, on the (010) mirror plane in monoclinic feldspars or near the plane in triclinic feldspars. All feldspars have topological monoclinic symmetry *C*2/*m* which can be lowered to *C*1 or *I*2/*c* in the fully *T*-ordered species.

Ordering at tetrahedral sites *T* causes an appearance of several polymorphs of potassic feldspar, ideally $K[AlSi_3O_8]$. Sanidine (*C*2/*m*) is a disordered species; if the Al content at *T*(1) is < 0.50 atoms per formula unit (*apfu*), the term high sanidine is used, while the variety with Al content at *T*(1) between 0.50 and 0.75 *apfu* is named low sanidine. In orthoclase, a pseudomonoclinic (pseudo-symmetry *C*2/*m*) due to microtwinning [with microtwinned triclinic (*C*1) domains] polymorph, the Al content at *T*(1) is > 0.75 *apfu*. Microcline (triclinic, *C*1) possesses an ordered structure with Al content at *T*10 + *T*1m in the range of 0.75–1.00 *apfu* [1,2,14,16,17]

2.1. Occurrence

The specimens with the new mineral were collected by us in July 2018 from the active Arsenatnaya fumarole situated at the summit of the Second scoria cone of the Northern Breakthrough of the Great Fissure Tolbachik Eruption of 1975–1976 (NB GFTE). This scoria cone is a monogenetic volcano about 300 m high and approximately 0.1 km^3 in volume that was formed in 1975 [18]. It is located 18 km SSW of the Ploskiy Tolbachik volcano in the central part of Kamchatka Peninsula, Far-Eastern Region, Russia. The description of the Arsenatnaya fumarole has been published by [19].

The temperature measured in the area during the collecting of samples with ferrisanidine was circa 400 °C. It is noteworthy that the sublimates of the Arsenatnaya fumarole contain rich silicate mineralization including feldspars. Sanidine–filatovite series members, Na-sanidine, anorthoclase and plagioclase (from andesine to anorthite) are quite common here [20,21]. Ferrisanidine is the rarest feldspar in this fumarole. It is associated with aegirine, cassiterite, hematite, sylvite, halite, johillerite, badalovite, arsmirandite, axelite, aphthitalite, litidionite, tridymite, polyarsite and evseevite.

3. Methods

The chemical composition of ferrisanidine was studied using electron microprobe. The analyses were carried out with a JEOL JXA-8230 instrument (WDS and EDS modes) at the Laboratory of Analytical Techniques of High Spatial Resolution, Dept. of Petrology, Moscow State University, Moscow, Russia. Standard operating conditions included an accelerating voltage of 20 kV and beam current of 10 nA, beam was rastered on an area of 4 μm × 4 μm. The data reduction was carried out by means of an INCA Energy 300 software package. The following standards were used for quantitative analysis: potassic feldspar (K), albite (Na), anorthite (Al and Si) and Fe (Fe). Contents of other elements with atomic numbers higher than carbon are below detection limits.

The Raman spectrum of ferrisanidine was recorded using an EnSpectr R532 spectrometer (Enhanced Spectrometry, Inc., Torrance, CA, USA) with a green laser (532 nm) at room temperature. The output power of the laser beam was about 7 mW. The spectrum was processed using the EnSpectr expert mode program (version PRO, Enhanced Spectrometry, Inc., Torrance, CA, USA) in the range from 100 to 4000 cm^{-1} with the use of a holographic diffraction grating with 1800 lines/cm and a resolution equals about 6 cm^{-1}. The diameter of the focal spot on the sample was about 10 μm. The Raman spectrum was acquired on a polycrystalline sample.

Single-crystal XRD studies of ferrisanidine could not be performed because of small size and imperfection (splitting and sponginess) of its crystals. The powder XRD data was obtain on the crushed small piece of ferrisanidine-aegirine aggregate (0.1–0.2 mm) using a Rigaku R-AXIS Rapid II diffractometer (Rigaku Corporation, Tokyo, Japan) equipped with a cylindrical image plate detector and rotating anode with the microfocus optics (Debye-Scherrer geometry; d = 127.4 mm; Co$K\alpha$ radiation). The raw powder XRD data were collected using the osc2xrd program suite designed by [22]. Calculated intensities were obtained by means of the STOE WinXPOW program (version 2.08, STOE & Cie GmbH, Darmstadt, Germany) suite based on the atomic coordinates and unit-cell parameters.

4. Results

4.1. Morphology, Physical Properties and Optical Data

Ferrisanidine forms porous, sometimes broken crusts up to 0.1 mm across and up to 20 μm thick composed by crude, cavernous short prismatic crystals (Figure 2a,b) or irregular in shape grains up to 10 μm × 20 μm. Another morphological variety of ferrisanidine (Figure 3) is represented by clusters of prismatic slightly split porous crystals overgrowing fine-grained cassiterite crusts. Ferrisanidine also occurs as thin single-crystal crusts epitaxially overgrowing crystals of sanidine (Figure 4).

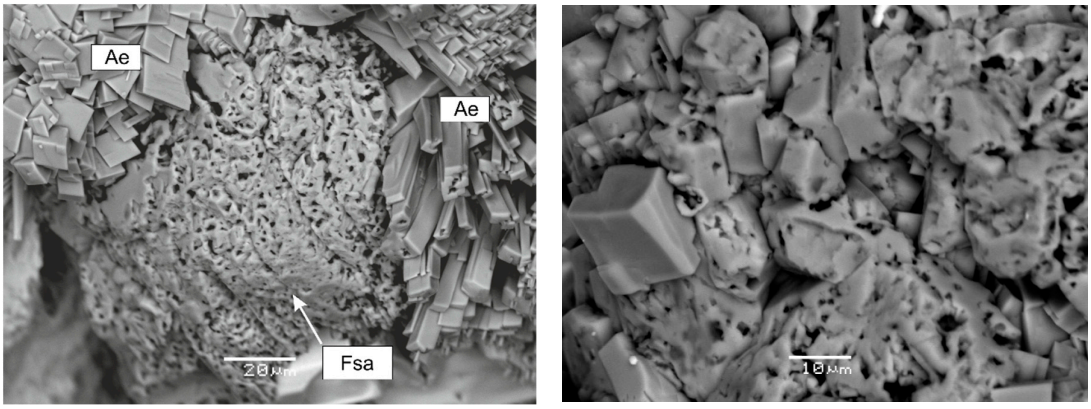

(**a**) (**b**)

Figure 2. (**a**) Spherical polymineralic aggregate (its cross-section is shown in Figure 3) covered by ferrisanidine (Fsa) crust with clusters of prismatic and pseudo-rhombohedral crystals of aegirine (Ae). SEM (SE mode) image. (**b**) Crust formed by crude, cavernous crystals of ferrisanidine (well-shaped short prismatic crystal in left part of the figure is aegirine). SEM (SE mode) image.

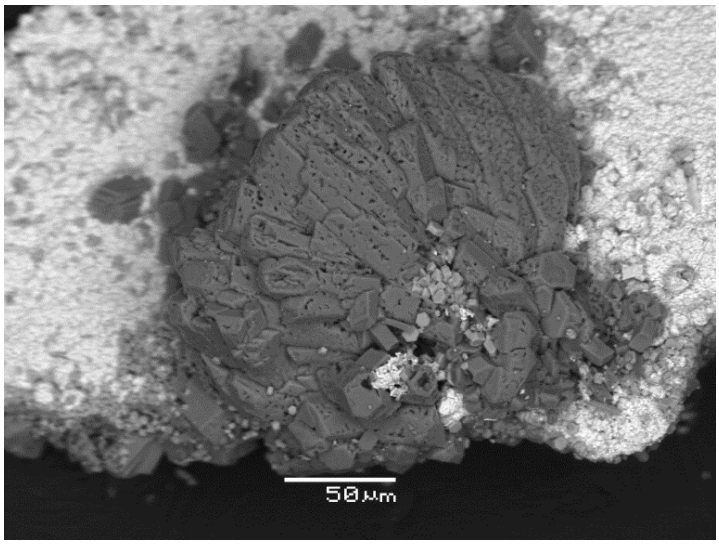

Figure 3. Radiating cluster of cavernous crystals of ferrisanidine on cassiterite (bright phase). SEM (BSE mode) image.

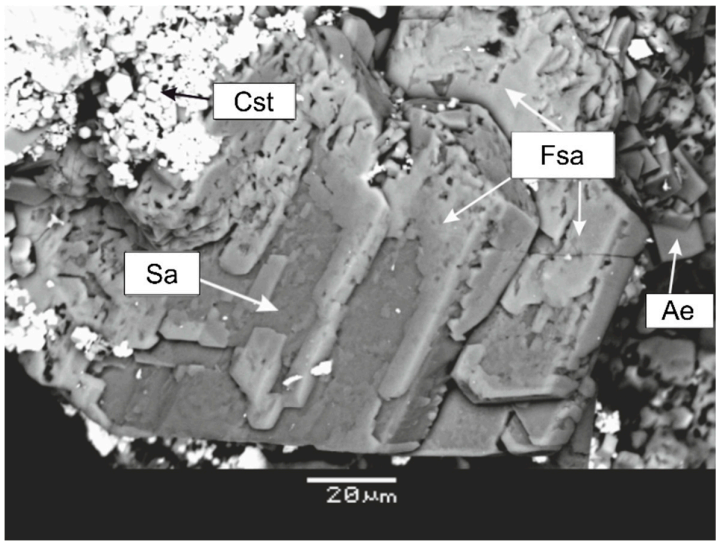

Figure 4. Ferrisanidine (Fsa) epitactically overgrowing crystals of sanidine (Sa) in association with cassiterite (Cst) and aegirine (Ae). SEM (BSE mode) image.

Ferrisanidine is transparent, colorless to white, with white streak. The lustre is vitreous. The mineral is brittle, perfect cleavage typical for feldspars was observed under the scanning electron microscope. Hardness and density could not be measured because crystals are tiny and aggregates are porous. The density value calculated from the empirical formula is 2.722 g·cm^{-3}.

Optical characteristics of ferrisanidine could not be correctly measured because of small size and porous character of crystals (Figures 2a,b and 5). Here, we give the data reported for the synthetic analogue of ferrisanidine by [8]. The superior, very low value of the Gladstone-Dale compatibility index [23] for ferrisanidine calculated using these refractive indices [1 − (K_P/K_c) = 0.002] indicates that these optical data correspond to the mineral well. The synthetic analogue of ferrisanidine is biaxial (–), α = 1.584(1), β = 1.595(1), γ = 1.605(1) (589 nm), 2V (meas.) = 85°, 2V(calc.) = 86.5°. Dispersion of optical axes was not observed. Orientation: $Y = b$, Z^c = 16(4)° [8]. Ferrisanidine is colorless and non-pleochroic under the microscope.

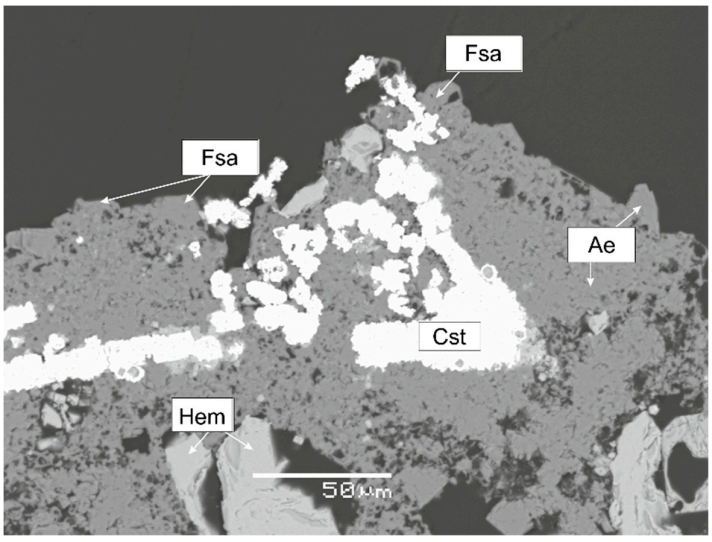

Figure 5. Ferrisanidine (Fsa) crystals forming interrupted crust which overgrows aggregate consisting of aegirine (Ae), cassiterite (Cst) and hematite (Hem). Polished section (the surface of such aggregate is shown in Figure 2a). SEM (BSE mode) image.

4.2. Chemical Data

Ferrisanidine possesses a rather stable chemical composition (Table 1).

Table 1. Chemical composition (in wt. %) of ferrisanidine.

Constituent	Mean*	Range	Standard. Deviation.
K_2O	15.15	15.11–15.18	0.03
Na_2O	0.25	0.20–0.32	0.04
Fe_2O_3	24.92	24.89–24.96	0.04
Al_2O_3	0.27	0.22–0.34	0.02
SiO_2	60.50	60.16–60.74	0.20
Total	101.09		

*Averaged for eight spot analyses.

No distinct impurities, such as P, As, Mg, Cu or Zn, which are inherent for Al-feldspars from the Arsenatnaya fumarole [20,21], were detected in ferrisanidine. The empirical formula of ferrisanidine calculated on the basis of 8 O *apfu* is $(K_{0.97}Na_{0.03})_{\Sigma 1.00}(Si_{3.03}Fe^{3+}_{0.94}Al_{0.02})_{\Sigma 3.99}O_8$. Thus, the new mineral is chemically close to the end-member with the idealized formula $K[Fe^{3+}Si_3O_8]$.

4.3. Raman Spectroscopy

The Raman spectra of ferrisanidine, sanidine, orthoclase and microcline have some common features but significantly differ from each other in number of bands and their positions (wavenumbers) [24,25] (Figure 6).

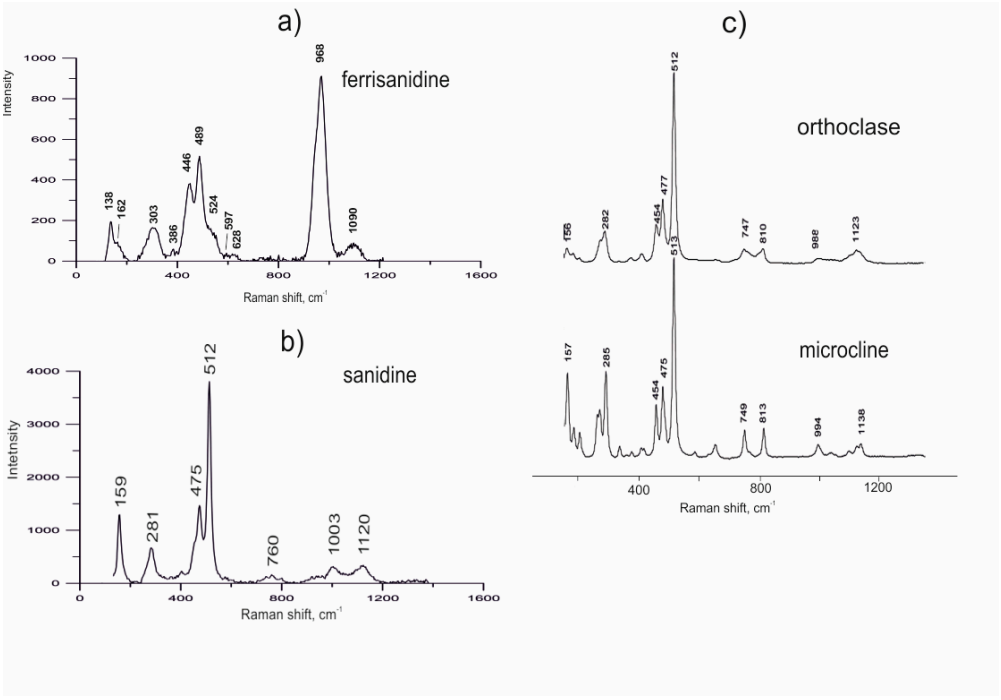

Figure 6. The Raman spectra of ferrisanidine from the Arsenatnaya fumarole (**a**) and sanidine from the extinct fumaroles of the Mountain 1004 (Tolbachik volcano) described in [21] (**b**); the Raman spectra of orthoclase and microcline given by [25] (**c**).

According to calculations, results of group analyses and vibrational studies undertaken by [24–26], there are several types of bands in the Raman spectra of feldspar-group minerals: Group I (450–520 cm^{-1})—strongest bands which belong to the ring-breathing modes of four-membered tetrahedral

rings; Group II (<300 cm^{-1})—bands corresponding to rotation-translation modes of the four-membered ring; Group III (300–450 cm^{-1})—cage-shear modes; Group IV (700–900 cm^{-1})—deformation modes of the tetrahedra; Group V (900–1200 cm^{-1})—vibrational stretching modes of the tetrahedra. Wavenumbers of distinct bands in the Raman spectrum of ferrisanidine (Figure 6a) are (cm^{-1}, s—strong band, sh—shoulder): 138s, 162sh, 303s, 386, 446s, 489s, 524sh, 597, 628, 968s, 1090. The shift of some bands in the Raman spectrum of ferrisanidine in the low-frequency range and high intensity of vibrational stretching bands of the tetrahedra united in four-membered rings (Group V), in comparison with the spectrum of sanidine (Figure 6b), are due to the presence of Fe^{3+} instead of Al in tetrahedrally coordinated sites of framework. The absence of strong bands related to the various modes of the $Fe^{3+}O_4$ tetrahedron (for example, at 730 cm^{-1}) in the shown spectra of ferrisanidine may be due to the orientation of crystals in aggregate of the studied sample.

4.4. Crystal Structure

The crystal structure of ferrisanidine was refined on a powder sample using the Rietveld method. Data treatment and the Rietveld structure analysis were carried out with the JANA software (version 2006, Institute of Physics, Praha, Czech Republic) [27]. A total of 13701 observed intensity envelope points were used in the refinement. The profiles of individual reflections were modeled using a Pseudo-Voigt function. The refinement of the crystal structure of ferrisanidine was complicated by the presence of admixed aegirine in the studied powder sample (Figure 7).

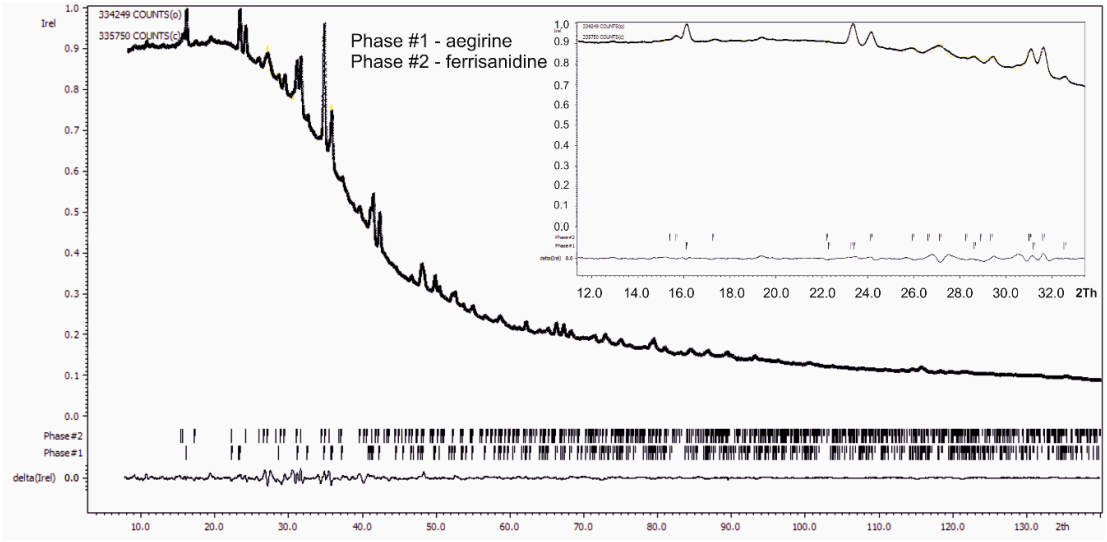

Figure 7. Rietveld refinement plot of mixture of ferrisanidine with aegirine. The models of synthetic AlFe-sanidine [12] (Phase #2; see Tables 5 and 6) and aegirine [28] (Phase #1) were used. Black graph is the experimental pattern of the mixture consisting of ferrisanidine and aegirine. The difference between the observed and calculated patterns is shown as a curve in the bottom part of the figure.

The most indicative reflections for both phases belong to the 2θ range 7.8–60° (Co$K\alpha$ radiation). The refined fraction of each phase, ferrisanidine and aegirine, in the mixture is 50%. As the initial model for the structure refinement of ferrisanidine we used the dataset on low AlFe-sanidine obtained by [12]. Unit-cell parameters of aegirine were refined using the structure model published by [28].

The comparative table including powder XRD patterns of ferrisanidine, its synthetic analogue and sanidine is given (Table 2).

Table 2. Powder X-ray diffraction data (*d* in Å) for ferrisanidine from Tolbachik, synthetic sanidine-type $K[Fe_{0.5}Al_{0.5}Si_3O_8]$ (FeAl-sanidine) and sanidine.

Ferrisanidine				Synthetic $K[Fe_{0.5}Al_{0.5}Si_3O_8]$ [12]		Sanidine [29]				
d_{meas}	I_{meas}	d_{calc}	I_{calc}	d_{calc}	I_{calc}	d_{calc}	I_{calc}	*h*	*k*	*l*
6.695	9	6.69	6	6.688	9	6.649	6	1	1	0
		6.572	1	6.615	1	6.446	2	0	0	1
6.574	23	6.571	25	6.551	13	6.518	10	0	2	0
5.961	9	5.966	11	5.912	7	5.865	9	1	1	−1
4.635*	7	4.647	5	4.619	1	4.583	2	0	2	1
4.283	**52**	4.281	62	4.262	56	4.234	58	2	0	−1
3.994	14	3.987	20	3.977	17	3.943	17	1	1	1
3.874	11	3.886	6	3.888	2	3.865	4	2	0	0
3.819	**36**	3.816	66	3.807	85	3.787	81	1	3	0
3.678	7	3.666	14	3.646	12	3.624	15	1	3	−1
3.589	7	3.587	12	3.572	11	3.551	13	2	2	−1
3.529	**30**	3.532	31	3.491	40	3.457	48	1	1	−2
3.346	**27**	3.348	34	3.313	58	3.284	55	2	0	−2
3.342*	**84**	3.345	84	3.344	100	3.325	100	2	2	0
3.285	**100**	3.286	100	3.257	77	3.223	78	0	0	2
		3.286	29	3.275	24	3.259	26	0	4	0
3.043	23	3.026	47	3.017	52	2.996	55	1	3	1
		2.983	24	2.956	10	2.932	8	2	2	−2
		2.939	9	2.916	12	2.889	11	0	2	2
2.939	**34**	2.939	20	2.926	21	2.908	24	0	4	1
2.822	2	2.821	1	2.815	1	2.798	1	3	1	−1
2.815	16	2.812	18	2.788	23	2.766	21	1	3	−2
2.643	**30**	2.645	23	2.626	20	2.607	20	3	1	−2
2.607*	16	2.607	29	2.597	31	2.583	34	2	4	−1
2.599	2	2.606	3	2.603	3	2.584	3	2	2	1
2.595	5	2.584	7	2.572	10	2.547	9	1	1	2
2.551*	57	2.542	11	2.543	10	2.528	10	3	1	0
2.515	2	2.509	3	2.505	3	2.492	4	2	4	0
2.481*	70	2.49	3	2.483	1	2.47	0	1	5	0
2.446*	9	2.447	7	2.437	8	2.423	8	1	5	−1
		2.424	1	2.395	1	2.371	0	2	0	−3
2.417*	2	2.411	10	2.405	10	2.392	10	3	3	−1
2.365*	5	2.367	5	2.341	4	2.316	6	1	1	−3
2.337*	2	2.345	1	2.329	0	2.316	0	2	4	−2
2.263*	11	2.324	1	2.309	0	2.292	0	0	4	2
		2.299	1	2.284	0	2.269	2	3	3	−2
		2.274	1	2.249	1	2.228	1	2	2	−3
2.225*	2	2.226	5	2.219	3	2.205	3	1	5	1
2.200*	**41**	2.191	29	2.183	21	2.172	23	0	6	0
2.136*	2	2.148	5	2.144	7	2.13	9	2	4	1
2.131	2	2.141	1	2.131	3	2.117	5	4	0	−2
2.103*	18	2.109	1	2.089	1	2.069	1	1	3	−3
2.093	2	2.092	1	2.087	1	2.068	2	2	0	2
2.076*	5	2.078	1	2.07	4	2.058	4	0	6	1
2.037*	18	2.036	6	2.026	12	2.014	12	4	2	−2
1.986*	11	1.994	8	1.988	11	1.972	11	2	2	2
1.983	2	1.989	1	1.971	2	1.955	3	3	3	−3
1.945	2	1.945	3	1.929	5	1.914	5	4	0	−3
1.942*	16	1.943	11	1.944	10	1.932	10	4	0	0
		1.908	1	1.903	2	1.894	2	2	6	0
1.889*	9	1.902	3	1.901	1	1.888	2	3	3	1
1.882	5	1.88	4	1.869	5	1.85	5	1	1	3

1.868	2	1.865	2	1.85	2	1.836	2	4	2	−3
1.866	2	1.864	2	1.864	2	1.853	2	4	2	0
1.846*	7	1.861	1	1.853	2	1.84	2	1	5	2
1.845	2	1.845	1	1.843	4	1.832	4	3	5	0
1.830*	16	1.834	15	1.812	18	1.792	20	2	0	−4
1.833	9	1.833	4	1.823	4	1.811	4	2	6	−2
1.825*	7	1.823	9	1.809	8	1.793	9	0	4	3
1.823**	14	1.823	11	1.814	8	1.801	8	0	6	2
1.812*	7	1.793	2	1.786	2	1.775	2	4	4	−2
1.792*	2	1.793	4	1.79	5	1.78	6	4	4	−1
1.763	2	1.765	3	1.759	3	1.747	4	2	4	2
1.735*	16	1.743	2	1.733	2	1.717	1	1	3	3
		1.72	2	1.714	1	1.704	2	5	1	−2
1.704	2	1.701	5	1.688	5	1.676	5	3	5	−3
1.672	5	1.671	2	1.663	3	1.652	3	1	7	−2
1.65	2	1.651	2	1.641	1	1.629	1	5	1	−3
		1.646	3	1.644	5	1.633	6	3	5	1
1.638*	20	1.643	1	1.637	1	1.629	1	0	8	0
1.617*	20	1.622	4	1.606	5	1.592	5	4	2	−4
1.597*	11	1.594	3	1.581	5	1.564	6	0	2	4
1.572	2	1.577	1	1.571	1	1.556	1	2	2	3
1.555	2	1.556	6	1.546	6	1.536	7	5	3	−3
1.545*	7	1.549	1	1.539	2	1.527	2	0	6	3
1.533*	9	1.531	2	1.525	1	1.519	7	4	6	−1
1.508	16	1.513	15	1.509	17	1.501	19	2	8	0
1.488*	2	1.48	1	1.471	2	1.46	2	1	7	−3
1.471*	9	1.475	2	1.468	1	1.459	1	2	8	−2
		1.471	1	1.459	1	1.445	1	1	5	−4
		1.47	2	1.461	3	1.446	4	1	1	4
		1.469	1	1.463	1	1.454	1	0	8	2
		1.465	2	1.465	3	1.456	3	5	3	0
1.454*	5	1.456	4	1.451	6	1.438	8	2	4	3
		1.454	2	1.445	2	1.436	2	4	6	−3
		1.453	2	1.452	2	1.444	2	4	6	0
1.451*	20	1.444	6	1.441	5	1.432	6	6	0	−2
		1.435	1	1.431	1	1.423	2	1	9	0
		1.428	1	1.428	1	1.414	1	3	5	2
		1.421	1	1.404	2	1.391	2	4	0	−5
1.42	5	1.419	5	1.418	6	1.407	7	4	0	2
		1.406	2	1.394	3	1.383	3	2	6	−4
		1.402	2	1.393	1	1.379	1	1	3	4

Note: For the calculated patterns, only reflections with intensities ≥1 are given. Indices *hkl* are given for ferrisanidine and, thus, the displacement of some reflections of synthetic $K[Fe_{0.5}Al_{0.5}Si_3O_8]$ and sanidine is due to the slight difference in *a:b:c* ratios. * Overlapped reflections of aegirine and ferrisanidine. The strongest reflections of ferrisanidine are marked in bold.

Data collection information and crystal structure refinement details for ferrisanidine are given in Table 3.

Table 3. Crystal data and Rietveld refinement details for ferrisanidine.

Formula	**$K[Fe^{3+}Si_3O_8]$**
Crystal system	Monoclinic
Space group	*C*2/*m*
a (Å)	8.678(4)
b (Å)	13.144(8)
c (Å)	7.337(5)
β (°)	116.39(8)
V (Å^3)	749.6(9)
Z	4
Radiation; wavelength (Å)	Co*Kα*1/ *α*2; 1.79021
Temperature (K)	293
F(000)	604
2*θ* range for data (°)	7.82 to 140.00
Profile function	Pseudo-Voight
Background function	36 Legendre polynoms
Goodness-of-fit on *F*	2.51
Final *R* indices	R_p = 0.0053, R_{wp} = 0.0075, R_1 = 0.0536, wR_2= 0.0678

Atomic scattering factors together with anomalous dispersion corrections were taken from International Tables for X-Ray Crystallography [30]. The final refinement cycles were finished with R_p = 0.0053, R_{wp} = 0.0075, R_1 = 0.0536, wR_2= 0.0678 and GOF = 2.51 for all data. Fractional atomic coordinates, refined site-scattering values and equivalent atomic displacement parameters (U_{eq}) are given in Table 4.

Table 4. Atom coordinates, site multiplicities (*Q*) and equivalent displacement parameters (U_{eq}, Å^2) of atoms and site occupancies for ferrisanidine.

Site	***x*/*a***	***y*/*b***	***z*/*c***	***U_{eq}**	***Q***	**Site Occupancy**
K1	0.2775(6)	0	0.1480(5)	0.061(2)	4	K
*T*1	0.0152(8)	0.1837(9)	0.2316(6)	0.020(4)	8	$Si_{0.72(15)}Fe_{0.28(15)}$
*T*2	0.7056(7)	0.1234(5)	0.3333(7)	0.035(3)	8	$Si_{0.74(13)}Fe_{0.26(13)}$
O1	0	0.1476(4)	0	0.080(6)	4	O
O2	0.6610(5)	0	0.2470(3)	0.019(4)	4	O
O3	0.8271(2)	0.1515(3)	0.2229(3)	0.034(1)	8	O
O4	0.0218(3)	0.3160(4)	0.2524(4)	0.054(3)	8	O
O5	0.1949(5)	0.1395(5)	0.4020(3)	0.062(2)	8	O

*U_{eq} is defined as one third of the trace of the orthogonalized U^{ij} tensor.

Selected interatomic distances in the ferrisanidine structure compared with data for synthetic low AlFe-sanidine [12] are presented in Table 5.

Table 5. Selected interatomic distances (Å) in the crystal structure of ferrisanidine and synthetic low AlFe-sanidine with the empirical formula $K_{0.98}[Fe_{0.51}Al_{0.48}]Si_{3.03}O_8$.

Central Atom	Coordinating Atom	Ferrisanidine	Synthetic AlFe-Sanidine
K(1)	O1 × 2	2.918(3)	2.932(3)
	O2	3.075(4)	2.767(5)
	O3 × 2	3.163(4)	3.065(4)
	O4 × 2	3.079(3)	3.140(4)
	O5 × 2	2.922(2)	2.979(4)
Mean, Å		<3.041>	<2.999>
Polyhedral volume, Å^3		50.467	44.285
T(1)	O1	1.705(2)	1.667(3)
	O3	1.660(2)	1.659(4)
	O4	1.744(2)	1.676(4)
	O5	1.612(3)	1.687(3)
Mean, Å		<1.680>	<1.672>
Polyhedral volume, Å^3		2.4	2.258
T(2)	O2	1.722(2)	1.642(2)
	O3	1.631(1)	1.639(4)
	O4	1.639(2)	1.638(3)
	O5	1.753(3)	1.641(3)
Mean, Å		<1.687>	<1.640>
Polyhedral volume, Å^3		2.402	2.239
Source		this work	[12]

5. Discussion

The primary goal of the crystal structure study of our new mineral was to identify the polymorph of $K[Fe^{3+}Si_3O_8]$.

The XRD study clearly demonstrates that our mineral is much closer to the most disordered potassic feldspar, sanidine rather to microcline. The comparison of calculated powder XRD patterns of ferrisanidine and microcline [21] is shown in Figure 8. The characteristic reflections that allow distinguishing these two minerals belong to the 2θ range 15–40°. In the powder XRD pattern of sanidine three the most important reflections inherent to microcline are absent, namely (*d*, Å–*I*, %; intensities *I* are given for Co$K\alpha$) 1–11 (5.926–5), 1–30 (3.705–46) and 1–31 (2.954–41).

Analysis of both powder XRD and Raman spectroscopic data shows that our new mineral from Tolbachik could not be considered as Fe-dominant analogue of orthoclase. The reasons are as follows: (1) the refined numbers of electrons in the *T* sites and *T*–O distances in tetrahedra show that Si and Fe^{3+} are disordered with Fe^{3+} at the *T*1 site <0.75, that corresponds to sanidine but not to orthoclase; (2) the Raman spectrum of orthoclase includes a well-resolved triplet in the region of 450–520 cm^{-1}, split bands in the 280–285 cm^{-1} region and resolved bands in the 745–820 cm^{-1} region (Figure 6), whereas the spectrum of ferrisanidine is closer to that of sanidine, which does not demonstrate such splitting of bands (Figure 6a). The comparison of sanidine and ferrisanidine is given in Table 6.

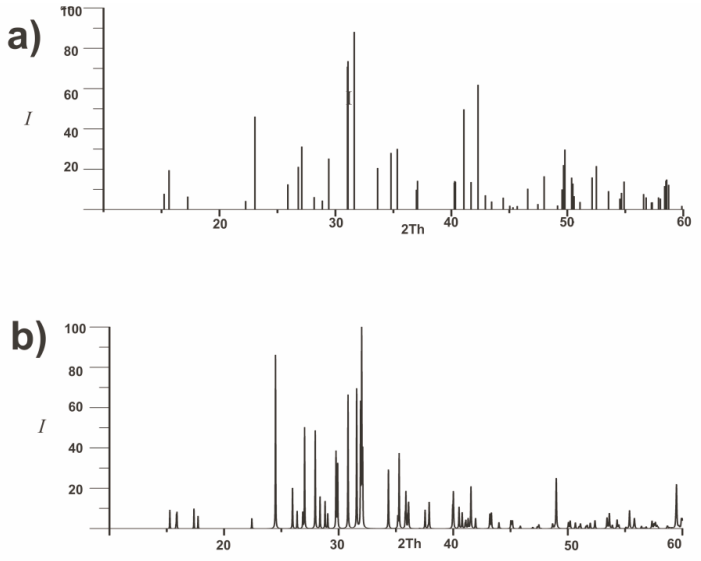

Figure 8. Powder X-ray diffraction patterns (Co*Kα*, bar charts) of ferrisanidine (**a**) and microcline (**b**), after [31], 2*θ* range 10–60°.

Table 6. Comparative data of sanidine and ferrisanidine.

Mineral	Sanidine	Ferrisanidine*
Formula	$K[AlSi_3O_8]$	$K[Fe^{3+}Si_3O_8]$
Crystal system	Monoclinic	Monoclinic
Space group	*C*2/*m*	*C*2/*m*
a, Å	8.54–8.60	8.678(4)
b, Å	13.00–13.04	13.144(8)
c, Å	7.17–7.20	7.337(5)
β, °	115.9–116.0	116.39(8)
V, Å^3	717.2–722.9	749.6(9)
Density, g cm^{-3}	2.56–2.60	2.722 (calc.)
Ten strongest reflections of the powder X-ray diffraction pattern: *d*, Å–*I*	4.234–58	6.571–25
	3.788–80	4.281–62
	3.458–47	3.816–66
	3.324–100	3.532–31
	3.283–55	3.348–34
	3.259–26	3.345–81
	3.223–77	3.286–100
	2.996–55	3.026–47
	2.908–23	2.607–29
	2.583–34	2.191–29
Optical data	Biaxial	Biaxial
α	1.519	1.584
β	1.523	1.595
γ	1.524	1.605
optical sign, 2*V*	(–) 0–60°	(–) 85°
References	[2,14,16,25]	This work; [8] for optical data

* Optical data are given for the synthetic analogue of ferrisanidine; the strongest reflections of a calculated powder XRD pattern of ferrisanidine are included.

The species diversity in the feldspar group is due mainly to the substitutions in the extra-framework cation sites and different schemes of Al/Si-ordering at tetrahedrally coordinated sites of the framework. Until this work, only two valid minerals of the feldspar group with species-defining tetrahedral components except of Si and Al were known, namely, the borosilicate reedmergnerite $Na[B^{3+}Si_3O_8]$ [32] and the alumino-arsenate filatovite $K[(Al,Zn)_2(As,Si)_2O_8]$ [33]. They are both very rare and known from few specific geological formations. Reedmergnerite occurs in dolomitic oil shales of the Green River formation in Utah, USA [32,34] and in peralkaline pegmatites of two alkaline complexes, Dara-i-Pioz in Tajikistan [4] and Lovozero at Kola peninsula, Russia [35]. Filatovite and intermediate members of the sanidine–filatovite solid-solution series are known only from sublimates of fumaroles at the Second scoria cone of the NB GFTE including the Arsenatnaya fumarole [20,33]. Ferrisanidine $K[Fe^{3+}Si_3O_8]$ is the second, after reedmergnerite $Na[B^{3+}Si_3O_8]$, natural feldspar without species-defining Al.

Different substitutions at framework sites are known in synthetic feldspars: Ga^{3+} (r_i = 0.47 Å), B^{3+} (r_i = 0.11 Å) and Fe^{3+} (r_i = 0.49 Å) substitute Al (r_i = 0.39 Å) whereas Ge^{4+} (r_i = 0.39 Å), P^{5+} (r_i = 0.17 Å) and As^{5+} (r_i = 0.34 Å) substitute Si (r_i = 0.26 Å) (the ionic radii are taken from [36]). These compounds were the focus of many studies. A lot of works were devoted to the various aspects of these phases: ways of synthesis, phase transitions, crystal chemical characteristics and physical properties [4,13,37,38]. However, the geochemistry of Ga and Ge do not facilitate an appearance of such feldspars in nature. Natural feldspars with species-defining P are also unknown; this component was reported in minerals of this group only as impurity: up to 5.0 wt. % P_2O_5 [21,39–44].

The crystal data of natural and synthetic Fe-rich sanidine-like feldspars are shown in Table 7. The unit-cell parameters of natural Fe-rich sanidine from Leucite Hills (Table 7) were obtained by selected-area electron diffraction (SAED) method [6]. The increase of Fe^{3+} content at tetrahedral sites affects the corresponding increase of all unit-cell parameters in the series $K[AlSi_3O_8]$–$K[Fe^{3+}Si_3O_8]$, which is clearly revealed on the powder XRD patterns in the increase of *d* values in this series (Table 2). This is the result of a substitution of Al for Fe^{3+}. Ferrisanidine is the only mineral in the feldspar group with a tetrahedrally coordinated component larger than Al^{3+}. The Si–O–Al connections in ferrisanidine are replaced by the Fe^{3+}–O–Si ones and in addition the Fe^{3+}–O–Fe^{3+} connections can appear, because of the Si/Fe^{3+} disorder at tetrahedral sites. It is known that feldspar-type crystal structures have a quite rigid framework. It constrains the free rotation of tetrahedra necessary for relaxation the strains due to the incorporation of different components (extra-framework and framework) [45]. One of the main indicators of the strain in silicates, e.g., feldspar-type crystal structures, is the average *T*–O–*T* angle, which is close to 140° for relaxed Si–O–Si [45]. This value slightly differs from the ideal one in different potassic feldspars, both natural and synthetic, with various tetrahedrally coordinated components. In sanidine the average *T*–O–*T* angle is 141.1° [29], in $K[GaSi_3O_8]$ 140.7° [46], in $K_{0.98}[(Fe^{3+}_{0.51}Al_{0.48})Si_{3.03}O_8]$ 141.3° [12]. The largest deviations are observed in the synthetic $K[AlGe_3O_8]$ 136.9° [47] and in ferrisanidine–137.5°. Both these feldspars have the largest unit-cell volumes: 801.7 and 749.6 $Å^3$, respectively. The strain in ferrisanidine and its synthetic analogues is caused by the more considerable mismatch of Fe^{3+} and Si size, than Al and Si, occupying the same sites. This is also the trigger for the highest ordering rate in $K[Fe^{3+}Si_3O_8]$ than in $K[AlSi_3O_8]$. As it was reported by [9], the phase transition from monoclinic $K[Fe^{3+}Si_3O_8]$ to triclinic polymorph happens at a temperature about 704 ± 6 °C, which is 200°C higher than for phase transition in $K[AlSi_3O_8]$. Moreover, the ordering kinetics in $K[Fe^{3+}Si_3O_8]$ is higher, than in synthetic $K[GaSi_3O_8]$ [13]. The "conservation" of disordered $K[Fe^{3+}Si_3O_8]$ in nature is rather surprising and proposed to be a quenched phase. We believe that ferrisanidine, similar to other silicates found in Tolbachik fumaroles, was deposited directly from the fumarolic gas as a volcanic sublimate at temperature range 500–700 °C [20].

The conditions of formation of silicates in Arsenatnaya and other oxidizing-type Tolbachik fumaroles (atmospheric pressure, temperature range 500–700 °C and transportation of chemical components by hot gas) are non-typical for geological settings ([19,20]. As our data show, sanidine, including its As^{5+}-bearing varieties, intermediate members of the sanidine-filatovite series, is a common mineral in fumarolic deposits of the Tolbachik volcano. However, the sanidine-filatovite

series feldspars are usually Fe-poor: <0.6 wt. % Fe_2O_3. Only in several specimens up to 3.4 wt. % Fe_2O_3 was detected [20]. Thus, no continuous solid-solution series between ferrisanidine and sanidine was found in the Tolbachik fumaroles. Moreover, the epitaxy of ferrisanidine on sanidine crystals (Figure 4) is an evident sign of their sequential crystallization with a break. The appearance of ferrisanidine $K[Fe^{3+}Si_3O_8]$, containing <0.3 wt. % Na_2O, in close association with aegirine $NaFe^{3+}[Si_2O_6]$ could be an indirect evidence of the instability of ferrious feldspars with higher content of sodium. The phase with chemical composition $NaFe^{3+}Si_3O_8$ is known only as a glass ([48,49]. The cause for preferable crystallization of potassic ferri-feldspar rather than sodic ferri-feldspar $NaFe^{3+}Si_3O_8$ probably has a crystal chemical nature. The framework composed of $Fe^{3+}O_4$ and SiO_4 tetrahedra is characterized by the significant elongation of *T*–O bonds and distortion of angles. This affects the *A*–O distances and, in general, the oxygen surrounding of extra-framework *A* cation. The Na^+ cation is smaller than K^+ and such irregular and distorted surrounding as it is not compatible with the feldspar structure with $[Fe^{3+}Si_3O_8]^-$ framework .

Table 7. Crystal data for ferrisanidine and other natural and synthetic Fe-rich sanidine-like feldspars.

Mineral/ Compound	**Ferrisanidine**	**Ferrisanidine (Al-Bearing Variety)***	**Fe-Sanidine**	**Low Fe-Sanidine**	**Low Fe-Sanidine**	**Low FeAl-Sanidine**	**Low AlFe-Sanidine**	**FeGe-Sanidine**
Formula	$K[Fe^{3+}Si_3O_8]$	$K_{0.96}Na_{0.04}[(Fe^{3+}_{0.70}Al_{0.20}Mg_{0.05}Ti_{0.03})Si_{3.02}O_8]$	$K[Fe^{3+}Si_3O_8]$	$K[Fe^{3+}Si_3O_8]$	$K[Fe^{3+}Si_3O_8]$	$K_{0.93}[(Al_{0.75}Fe^{3+}_{0.27})Si_{3.01}O_8]$	$K_{0.98}[(Fe^{3+}_{0.51}Al_{0.48})Si_{3.03}O_8]$	$K[Fe^{3+}Ge_3O_8]$
Crystal system	Monoclinic							
Space group	*C*2/*m*							
a (Å)	8.678(4)	8.68(15)	8.68	8.689(2)	8.687(3)	8.627(4)	8.655(7)	8.891(2)
b (Å)	13.144(8)	13.14(23)	13.12	13.16(2)	13.144(2)	13.058(3)	13.101(9)	13.703(1)
c (Å)	7.337(5)	7.31(15)	7.31	7.239(2)	7.282(2)	7.209(3)	7.250(8)	7.542(2)
β (°)	116.39(8)	116.00(46)	116.06	116.07(1)	115.97(2)	116.00(2)	116.02(2)	115.86(2)
V (Å^3)	749.6(9)	749.3(1)	749.3(2)	749.0(4)	747.5(5)	730.0(7)	738.7(1)	826.9(3)
Origin	natural	natural	synthetic	synthetic	synthetic	synthetic	synthetic	synthetic
References	This work	[6]	[8]	[14]	[10]	[11]	[12]	[50]

* Originally described as "Fe-rich sanidine" by [5].

Author Contributions: N.V.S. and I.V.P. wrote the paper. N.V.S. carried out the crystal structure analysis. N.V.S. and S.N.B. obtained and processed X-ray diffraction data. N.N.K. and M.F.V. obtained and processed electron microprobe and Raman spectroscopic data. I.V.P and E.G.S. collected and prepared samples.

Funding: This work was supported by the Russian Science Foundation, grant No. 19-17-00050.

Acknowledgements: We are grateful to Vasiliy O. Yapaskurt for his assistance in the SEM studies. We thank our anonymous reviewers for their valuable comments. Powder XRD study was carried out with the technical support by the SPbSU X-Ray Diffraction Resource Center.

Conflicts of Interest: The authors declare no conflict of interest.

References

1. Deer, W.A.; Howie, R.A.; Zussman, J. *Rock-Forming Minerals. Framework Silicates: Feldspars*, 2nd ed.; Geological Society: London, UK, 2001.
2. Bokiy, G.B.; Borutsky, B.E. *Minerals. Reference Book Vol. V: Tectosilicates. Pt. 1: Silicates with Interrupted Frameworks and Feldspars*; Nauka Publishing: Moscow, Russia, 2003. (In Russian)
3. Lacroix, A. Note pre´liminaire sur quelques mine´raux de Madagascar dont plusieurs peuvent tre utilise´s comme gemmes. *Comptes Rendus l'Academie Sci. Paris* **1912**, *155*, 672–677.
4. Grew, E.S.; Yates, M.G.; Belakovskiy, D.I.; Rouse, R.C.; Su, S.C.; Marquez, N. Hyalotekite from reedmergnerite-bearing peralkaline pegmatite, Dara-i-Pioz, Tajikistan and from Mn skarn, Långban, Värmland, Sweden: A new look at an old mineral. *Miner. Mag.* **1994**, *58*, 285–297.
5. Linthout, K.; Lustenhouwer, W. Ferrian high sanidine in a lamproite from Cancarix, Spain. *Miner. Mag.* **1993**, *57*, 289–299.
6. Kuehner, S.M.; Joswiak, D.J. Naturally occurring ferric iron sanidine from the Leucite Hills lamproite. *Am. Mineral.* **1996**, *81*, 229–237.
7. Faust, G.T. The fusion relations of ironorthoclase, with a discussion of the evidence of the existence of an iron-orthoclase molecule in feldspars. *Am. Mineral.* **1936**, *21*, 735–763.
8. Wones, D.R.; Appleman, D.E. X-ray crystallography and optical properties of synthetic monoclinic $KFeSi_3O_8$, iron-sanidine. *USA Geol. Surv. Prof. Paper* **1961**, *424-C*, 309–310.
9. Wones, D.R.; Appleman, D.E. Properties of synthetic triclinic $KFeSi_3O_8$, iron-microcline, with some observations on the iron-microcline ≒ iron-sanidine transition. *J. Petrol.* **1963**, *4*, 131–137.
10. Bychkov, A.M.; Rusakov, V.S.; Kuz'mina, N.A.; Khramov, D.A.; Urusov, V.S. Ferrisilicate feldspars and feldspathoids: Synthesis, X-ray and Mössbauer spectroscopy data. *Geokhimiya* **1995**, *11*, 1600–1615. (In Russian)
11. Nadezhina, T.N.; Pushcharovsky, D.Y.; Taroev, V.K.; Tauson, V.L.; Bychkov, A.M. Crystal structure of a low sanidine ferroalumosilicate. *Crystallogr. Rep.* **1993**, *38*, 753–758.
12. Lebedeva, Y.S.; Pushcharovsky, D.Y.; Pasero, M.; Merlino, S.; Kashaev, A.A.; Taroev, V.K.; Göttlicher, J.; Kroll, H.; Pentinghaus, H.; Suvorova, L.F.; et al. Synthesis and crystal structure of low ferrialuminosilicate sanidine. *Crystallogr. Rep.* **2003**, *48*, 919–924.
13. Taroev, V.; Göttlicher, J.; Kroll, H.; Kashaev, A.; Suvorova, L.; Pentinghaus, H.; Bernotat-Wulf, H.; Breit, U.; Tauson, V.; Lashkevich, V. Synthesis and structural state of K-feldspars in the system $K[AlSi_3O_8]$–$K[FeSi_3O_8]$. *Eur. J. Miner.* **2008**, *20*, 635–651.
14. Smith, J.V. *Feldspar Minerals. II. Crystal Structure and Physical Properties*; Springer: Berlin, Germany, 1974.
15. Kroll, H.; Ribbe, P.H. Lattice parameters, composition and Al, Si order in alkali feldspars. *Rev. Mineral.* **1983**, *2*, 57–99.
16. Parsons, I. *Feldspars and Their Reactions: Proceedings of the NATO Advanced Study Institute on Feldspars and Their Reactions*; Springer: Edinburgh, UK, 1994.
17. McConnel, J.D.C. Electron-optical study of phase transformations. *Miner. Mag.* **1971**, *38*, 1–20.
18. Fedotov, S.A.; Markhinin, Y.K. *The Great Tolbachik Fissure Eruption;* Cambridge University Press: Cambridge, UK, 1983.
19. Pekov, I.V.; Koshlyakova, N.N.; Zubkova, N.V.; Lykova, I.S.; Britvin, S.N.; Yapaskurt, V.O.; Agakhanov, A.A.; Shchipalkina, N.V.; Turchkova, A.G.; Sidorov, E.G. Fumarolic arsenates—A special type of arsenic mineralization. *Eur. J. Miner.* **2018**, *30*, 305–322.

20. Shchipalkina, N.V.; Pekov, I.V.; Koshlyakova, N.N.; Sidorov, E.G. Silicate mineralization from sublimates of the Arsenatnaya fumarole (Tolbachik volcano, Kamchatka, Russia). In Proceedings of the XXXVI International Conference on Magmatism of the Earth and Related Strategic Metal Deposits, St. Petersburg, Russia, 23–26 May 2019.
21. Shchipalkina, N.V.; Pekov, I.V.; Britvin, S.N.; Koshlyakova, N.N.; Sidorov, E.G. Arsenic and phosphorus in feldspar framework: Sanidine–filatovite solid-solution series from fumarolic exhalations of the Tolbachik volcano, Kamchatka, Russia. *Phys. Chem. Miner.* **2019**, doi:10.1007/s00269-019-01067-5.
22. Britvin, S.N.; Dolivo-Dobrovolsky, D.V.; Krzhizhanovskaya, M.G. Software for processing the X-ray powder diffraction data obtained from the curved image plate detector of Rigaku RAXIS Rapid II diffractometer. *Zap. RMO* **2017**, *146*, 104–107. (In Russian)
23. *Mandarino,* J.A. The Gladstone-Dale relationship; Part IV, The compatibility concept and its application. *Can. Miner.* **1981**, *19*, 441–450.
24. Bendel, V.; Schmidt, B.C. Raman spectroscopic characterisation of disordered alkali feldspars along the join $KAlSi_3O_8$–$NaAlSi_3O_8$: Application to natural sanidine and anorthoclase. *Eur. J. Miner.* **2008**, *20*, 1055–1065.
25. Freeman, J.J.; Wang, A.; Kuebler, K.E.; Jolliff, B.L.; Haskin, L.A. Characterization of natural feldspars by Raman spectroscopy for future planetary exploration. *Can. Miner.* **2008**, *46*, 1477–1500.
26. McKeown, D.A. Raman spectroscopy and vibrational analyses of albite: From 25 °C through the melting temperature. *Am. Miner.* **2005**, *90*, 1506–1517.
27. *Petříček*, V.; Dušek, M.; Palatinus, L. *Jana 2006. Structure Determination Software Programs*; Institute of Physics: Praha, Czech, 2016.
28. Nestola, F.; Tribaudino, M.; Boffa Ballaran, T.; Liebske, C.; Bruno, M. The crystal structure of pyroxenes along the jadeite—hedenbergite and jadeite—aegirine joins. *Am. Miner.* **2007**, *92*, 1492–1501.
29. Ferguson, R.B.; Ball, N.A.; Cerny, P. Structure refinement of an adularian end-member high sanidine from the Buck Claim pegmatite, Bernic Lake, Manitoba. *Can. Miner.* **1991**, *29*, 543–552.
30. Ibers, J.A.; Hamilton, W.C. *International Tables for X-ray Cristallography: Revised and Supplementary Tables*; Kynoch Press: Birmingham, UK, 1974.
31. Finney, J.J.; Bailey, S.W. Crystal structure of an authigenic maximum microcline. *Z. Kristallogr.* **1997**, *119*, 413–436.
32. Milton, C.; Chao, E.C.T.; Axelrod, J.M.; Grimaldi, F.S. Reedmergnerite, $NaBSi_3O_8$, the boron analogue of albite, from the Green River formation, Utah. *Am. Miner.* **1960**, *45*, 188–199.
33. Vergasova, L.P.; Krivovichev, S.V.; Britvin, S.N.; Burns, P.C.; Ananiev, V.V. Filatovite, $K[(Al,Zn)_2(As,Si)_2O_8]$, a new mineral species from the Tolbachik volcano, Kamchatka peninsula, Russia. *Eur. J. Miner.* **2004**, *16*, 533–536.
34. Milton, C. Green River mineralogy. In *Mineralogy. Encyclopedia of Earth Science*; Springer: Boston, MA, USA, 1981.
35. Khomyakov, A.P. *Mineralogy of Hyperagpaitic Alkaline Rocks*; Clarendon Press: Oxford, UK, 1995.
36. Shannon, R.D. Revised effective ionic radii and systematic studies of interatomic distances in halides and chalcogenides. *Acta Cryst.* **1969**, *A32*, 751–767.
37. Fleet, M.E. Tetrahedral-site occupancies in reedmergnerite and synthetic boron albite ($NaBSi_3O_8$). *Am. Miner.* **1992**, *77*, 76–84.
38. Kotelnikov, A.R.; Shchipalkina, N.V.; Suk, N.I.; Ananiev, V.V. Synthesis of As-Bearing Feldspar. In Proceedings of the X International Symposium "Mineral Diversity: Research and Preservation", Sofia, Bulgaria, 14–16 October 2019.
39. London, D.; Cerny, P.; Loomis, J.L.; Pan, J.J. Phosphorus in alkali feldspars of rare-element granitic pegmatites. *Can. Miner.* **1990**, *28*, 771–786.
40. London, D.; Wolf, M.B.; Morgan, G.B.; Garrido, M.G. Experimental silicate-phosphate equilibria in peraluminous granitic magmas, with a case study of the Alburquerque batholith at Tres Arroyos Badajoz, Spain. *J. Petrol.* **1999**, *40*, 215–240.
41. London, D. Phosphorus in S-type magmas: The P_2O_5 content of feldspars from peraluminous granites, pegmatites and rhyolites. *Am. Miner.* **1992**, *77*, 126–145.
42. Fryda, J.; Breiter, K. Alkali feldspars as a main phosphorus reservoirs in rare-metal granites: Three examples from the Bohemian massif (Czech Republic). *Terra Nova* **1995**, *7*, 315–320.
43. Kontak, D.J.; Martin, R.F.; Richard, L. Patterns in phosphorus enrichment in alkali feldspar, South Mountain batholith, Nova Scotia, Canada. *Eur. J. Miner.* **1996**, *8*, 805–824.

44. Broska, I.; Williams, C.T.; Uher, P.; Konecny, P.; Leichmann, J. The geochemistry of phosphorus in different granite suites of the Western Carpathians, Slovakia: The role of apatite and P-bearing feldspar. *Chem. Geol.* **2004**, *205*, 1–15.
45. Liebau, F. *Structural Chemistry of Silicates*; Springer: Berlin, Germany, 1985.
46. Kimata, M.; Saito, S.; Shimizu, M. Structure of sanidine-type $KGaSi_3O_8$: Tetrahedral disordering in potassium feldspar. *Eur. J. Miner.* **1995**, *7*, 287–293.
47. Kroll, H.; Floegel, J.; Breit, U.; Loens, J.; Pentinghaus, H. Order and anti-order in Ge-substituted alkali feldspars. *Eur. J. Miner.* **1991**, *3*, 739–749.
48. Henderson, G.S.; Fleet, M.E.; Bancroft, G.M. An x-ray scattering study of vitreous $KFeSi_3O_8$ and $NaFeSi_3O_8$ and reinvestigation of vitreous SiO_2 using quasi-crystalline modelling. *J. Non-Cryst. Solids* **1984**, *68*, 333–349.
49. Marcial, J.; Ahmadzadeh, M.; McCloy, J.S. Effect of Li, Fe, and B addition on the crystallization behavior of sodium aluminosilicate glasses as analogues for Hanford high level waste glasses. *MRS Adv.* **2017**, *10*, 549–555.
50. Pentinghaus, H.; Bambauer, H.U. Substitution of A1(III), Ga(III), Fe (III)and Si(IV), Ge(IV) in synthetic alkali feldspars. *N. Jb. Miner. Mh.* **1971**, 416–418.